On The Design of Nonlinear PID Controller for Nonlinear Quadrotor System

Aws Abdulsalam Najm, Ibraheem Kasim Ibraheem Elect. Eng. Dept. / College of Eng. / Baghdad University, 10001, Baghdad, Iraq

Abstract

A nonlinear PID controller is proposed to stabilize the motion of a 6-DOF quadrotor and enforce it to track a given trajectory with minimum energy and error. We used the complete nonlinear model of the quadrotor in the design process, taking into account the velocity and acceleration vectors to keep the quadrotor model more accurate and close to the actual system. The asymptotic stability of the closed-loop system is proved using Lyapunov stability theorem under certain conditions. The simulations have been accomplished under MATLAB environment and included three different trajectories, i.e., circular, helical, and square. The proposed nonlinear PID controller has been compared with the linear PID one and the simulations showed the effectiveness of the proposed nonlinear PID controller in terms of speed, control energy, and steady-state error.

Keywords:UAV, Quadrotor, Nonlinear PID, Lyapunov stability, linear position vector, closed-loop, circular trajectory.

1 Introduction

A quadrotor is one of the unmanned aerial vehicles (UAV), it does not need a pilot to be controlled. Quadrotor has four arms each one has a rotor on it. Every two rotors on the same axis rotate in the same direction and opposite to the other two rotors direction of rotation. The quadrotor is underactuated system, because the number of rotors is less than the number of DOF. This makes designing a controller is a difficult problem. Quadrotors applications have been increased in the last years because of their simple implementation, low cost, different sizes, and maneuverability. Many applications founded for danger places, disasters, and rescue [1-3]. [4] and [5] are the quadrotor applications in agriculture, and even in helpful jobs like [6] and [7]. The work in [8] is a good survey for quadrotor applications for entertainment. Many studies could be found for the multi-agent system and formation control like [9–11], and for more applications in multi-agent systems we recommend [12]. Many researchers study the quadrotor control design with different types of controllers. One of the most used controllers is the linear PID control because of its simplicity [13–16] but on the other hand it has many disadvantages: 1) sometimes it gives a high control signal due to the fact of windup, thus, overshooting and continuing to increase as this accumulated error is unwound (offset by errors in the other direction, 2) the differentiator leads to noise amplification. Other used controllers like: Nonlinear PID control [17] and [18], LQR [19], geometric control [20], nonlinear model predictive control [21], L1 control [22], fuzzy control [23] and [24], A further search for control algorithms with quadrotor can be found [25].

In this paper, a nonlinear PID controller proposed in our previous work [26], it is a combination of nonlinear functions of the error signal and used to stabilize a 6-DOF quadrotor system, its stability using Lyapunov techniques is investigated, and compare its performance with most famous one, the linear PID controller. The control system for the 6-DOF UAV with proposed controller consists of six nonlinear PID controllers, three nonlinear PID controllers for the translational system and another

three ones for the rotational system of the underlying UAV. With twelve tuning parameters for each controller. These parameters have been tuned using GA and optimized toward the minimization of the proposed performance index.

The structure of this paper is as follows: Section 2 describes the problem statement. Next, Section 3 presents the exact nonlinear modeling of the quadrotor. The nonlinear controller design and stability analysis are the main results and given in Section 4. Section 5 illustrates the numerical simulations and discussions followed by a conclusion and future work in Section 6.

2 Problem statement

Suppose that the equations below represent the nonlinear 6-DOF quadrotor system shown in Fig. 1:

$$\begin{cases} X^{n} = F(X, \dot{X}, ..., X^{n-2}, X^{n-1}) + G(X)U \\ Y = X \end{cases}$$
 (1)

Where: $X \in \mathbb{R}^n$ is Linear and angular position vectors of the quadrotor system, $Y \in \mathbb{R}^n$ is the measured output of the plant, in the underlying quadrotor system, it is the vector $X, U \in \mathbb{R}^n$ is the control input vector of the quadrotor system which needs to be designed such that it stabilizes the unstable 6-DOF quadrotor system and makes it follows a specific trajectory subject to optimum timedomain specifications and minimum control energy.

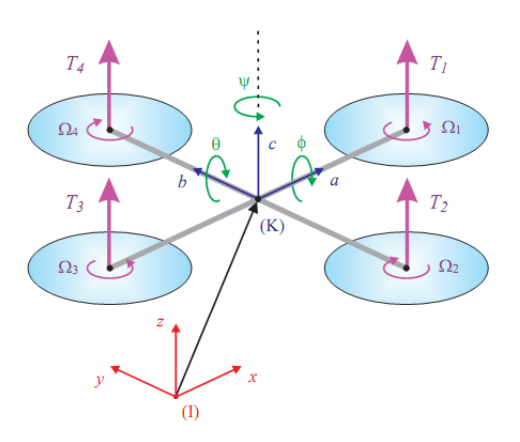


Figure 1: Quadrotor System

3 Mathematical Modelling of the 6-DOF UAV Quadrotor

To control any system, firstly, a mathematical model must be derived. This mathematical model will describe the responses of the system for different inputs. The inputs for the quadrotor are combinations of the rotors speed (Ω) , which in this case is a force f_t to control the altitude (z) and the torques $(\tau_x, \tau_y, \text{ and } \tau_z)$ to control the angels (ϕ, θ, τ_z) and ψ), see (2), the meaning of each parameter is described in Table 1.

$$\begin{cases}
f_t = b(\Omega_1^2 + \Omega_2^2 + \Omega_3^2 + \Omega_4^2) \\
\tau_x = bl(\Omega_3^2 - \Omega_1^2) \\
\tau_y = bl(\Omega_4^2 - \Omega_2^2) \\
\tau_z = d(\Omega_2^2 + \Omega_4^2 - \Omega_1^2 - \Omega_3^2))
\end{cases} (2)$$

Table 1: Parameters Description

Parameters	Description	Units	
[x y z]	Linear position vector	m	
$[\phi \theta \psi]$	Angular position vector	rad	
[uvw]	Linear velocity vector	m/sec	
[pqr]	Angular velocity vector	rad/sec	
$[I_x I_y I_z]$	Moment of inertia vector	$kg.m^2$	
f_t	Total thrust generated by rotors	N	
$[\tau_x \tau_y \tau_z]$	Control torques	N.m	
$[f_{wx} f_{wy} f_{wz}]$	Wind force vector	N	
$[\tau_{wx}\tau_{wy}\tau_{wz}]$	Wind torque vector	N.m	
g	Gravitational force	m/sec^2	
\overline{m}	Total mass	Kg	
$[\Omega_1 \Omega_2 \Omega_3 \Omega_4]$	Rotors speeds vector	rad/sec	
b	Thrust coefficient	$N.sec^2$	
l	Motor to center length	m	
d	Drag coefficient	$N.m.sec^2$	
$c() \equiv cos(), s() \equiv sin(), and t() \equiv tan()$			

The four possible movements of the quadrotor are shown in Fig. 2. Some researchers [13–15], and [27] depend only on the equations of acceleration for the quadrotor without taking the velocities into account. The mathematical model in this paper takes the acceleration and velocity vectors into considerations to make this model more accurate and close to the actual system. The nonlinear mathematical model equations of the 6-DOF quadrotor are shown in (3)[28]. Fig. 3 shows the block diagram of the quadrotor dynamical relations.

$$\begin{cases}
\begin{pmatrix} \dot{x} \\ \dot{y} \\ \dot{z} \end{pmatrix} = \begin{pmatrix} c(\psi)c(\theta) & [c(\psi)s(\phi)s(\theta) - c(\phi)s(\psi)] & [s(\phi)s(\psi) + c(\phi)c(\psi)s(\theta)] \\ c(\theta)s(\psi) & [c(\phi)c(\psi) + s(\phi)s(\psi)s(\theta)] & [c(\phi)s(\psi)s(\theta) - c(\psi)s(\phi)] \end{pmatrix} \begin{pmatrix} u \\ v \\ -s(\theta) & c(\theta)s(\phi) & c(\phi)c(\theta) \end{pmatrix} \\
\begin{pmatrix} \dot{u} \\ \dot{v} \\ \dot{w} \end{pmatrix} = \begin{pmatrix} 0 & r & -q \\ -r & 0 & p \\ q & -p & 0 \end{pmatrix} \begin{pmatrix} u \\ v \\ w \end{pmatrix} + g \begin{pmatrix} -s(\theta) \\ s(\phi)c(\theta) \\ c(\phi)c(\theta) \end{pmatrix} + \frac{1}{m} \begin{pmatrix} f_{wx} \\ f_{wy} \\ f_{wz} - f_t \end{pmatrix} \\
\begin{pmatrix} \dot{\phi} \\ \dot{\theta} \\ \dot{\psi} \end{pmatrix} = \begin{pmatrix} 1 & s(\phi)t(\theta) & c(\phi)t(\theta) \\ 0 & c(\phi) & -s(\phi) \\ 0 & \frac{s(\phi)}{c(\theta)} & \frac{c(\phi)}{c(\theta)} \end{pmatrix} \begin{pmatrix} p \\ q \\ r \end{pmatrix} \\
\begin{pmatrix} p \\ q \\ r \end{pmatrix} = \begin{pmatrix} \frac{I_y - I_z}{I_x} \\ \frac{I_z - I_y}{I_z} \\ \frac{I_x - I_y}{I_z} \end{pmatrix} \begin{pmatrix} rq \\ pr \\ pq \end{pmatrix} + \begin{pmatrix} \frac{\tau_x + \tau_{wx}}{I_x} \\ \frac{\tau_y + \tau_{wz}}{I_y} \\ \frac{\tau_z + \tau_{wz}}{I_z} \end{pmatrix}
\end{cases} (3)$$

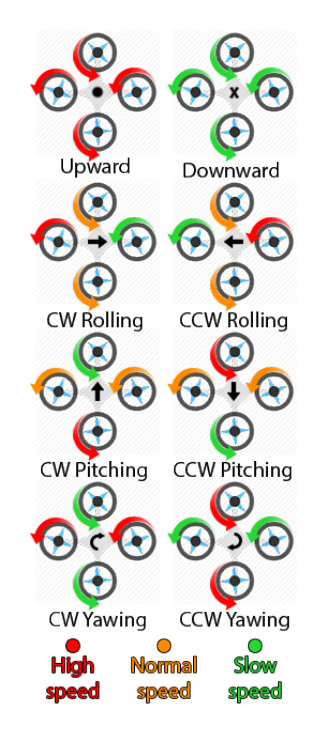


Figure 2: Possible Movements

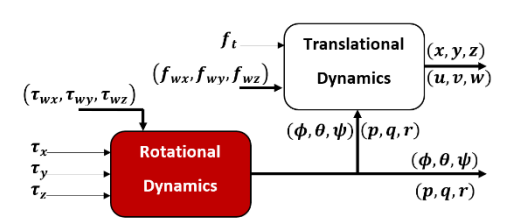


Figure 3: Quadrotor Dynamics Relations

Our mathematical model is based on Newton and Euler equations to represent the 3D motion of the rigid body [28, 29]. To control the quadrotor in the 6-DOF, a combination of translational (x,y,z) and rotational (ϕ,θ,ψ) motions is needed. From Newtons law [28]:

$$\begin{pmatrix} \ddot{x} \\ \ddot{y} \\ \ddot{z} \end{pmatrix} = -\frac{f_t}{m} \begin{pmatrix} s(\phi)s(\psi) + c(\phi)c(\psi)s(\theta) \\ c(\phi)s(\psi)s(\theta) - c(\psi)s(\phi) \\ c(\phi)c(\theta) \end{pmatrix} + \begin{pmatrix} 0 \\ 0 \\ g \end{pmatrix}$$
(4)

4 The main results

4.1 Nonlinear Controller Design

The Linear PID controller is a linear combination of the gains (K_p, K_d, K_i) (5). The Nonlinear PID controller replaces each gain with a nonlinear function of the error signal so as to get a more satisfactory response for the nonlinear 6-DOF quadrotor system. In addition, less control energy and good disturbance rejection are obtained with the nonlinear PID control while the error is changing continuously. Furthermore, the error signal itself is replaced by a nonlinear function f(e). Our nonlinear PID controller is proposed in with little modification in the integral term of (6), where the term k_{i1} is added to increase the stability of the closed-loop system.

$$U_{PID} = K_p e + K_d \dot{e} + K_i \int e \, dt \tag{5}$$

$$\begin{cases} U_{NLPID} = f_1(e) + f_2(\dot{e}) + f_3(\int e \, dt) \\ f_i(\beta) = \left(k_{i1} + \frac{k_{i2}}{1 + exp(\mu_i \beta^2)}\right) |\beta|^{\alpha_i} sign(\beta) \end{cases}$$
(6)

Where: β could be e, \dot{e} , or $\int e \, dt$, and i=1,2, and 3. Quadrotor controlling algorithm must be divided into two parts because of the under actuated phenomena. The First part is where the input control is available, it is called the Inner-Loop Control(ILC). While the second part is where there is no actual input control available and it is called the Outer-Loop Control(OLC).

4.1.1 Nonlinear design for ILC

The proposed control signals for the altitude z and the attitude $(\phi, \theta, \text{ and } \psi)$ motions are given as follows,

The throttle force control f_t :

$$U_z = f_t = f_1(e_z) + f_2(\dot{e}_z) + f_3(\int e_z \, dt)$$

$$e_z = z_{desired} - z_{sensor}$$
(7)

While the Roll torque control signal τ_x :

$$U_{\phi} = \tau_x = f_1(e_{\phi}) + f_2(\dot{e}_{\phi}) + f_3(\int e_{\phi} dt)$$

$$e_{\phi} = \phi_{desired} - \phi_{sensor}$$
(8)

The Pitch torque control signal τ_y :

$$U_{\theta} = \tau_{y} = f_{1}(e_{\theta}) + f_{2}(\dot{e}_{\theta}) + f_{3}(\int e_{\theta} dt)$$

$$e_{\theta} = \theta_{desired} - \theta_{sensor}$$
(9)

Finally, the Yaw torque control τ_z :

$$U_{\psi} = \tau_z = f_1(e_{\psi}) + f_2(\dot{e}_{\psi}) + f_3(\int e_{\psi} dt)$$

$$e_{\psi} = \psi_{desired} - \psi_{sensor}$$
(10)

Where: subscript "sensor" means the measured values from different sensors of the quadrotor system.

4.1.2 Nonlinear design for OLC

Quadrotor system has no control input for the motion in the (x, y) plane, the following analysis is proposed to generate the appropriate control signals $(U_x \text{ and } U_y)$ for the motion in the (x, y) plane, see (4). Simplifying the model of (4) by assuming the ϕ and θ angle deviations are small (i.e. β is small $\Rightarrow c(\beta) = 1, s(\beta) = \beta$).

$$\begin{pmatrix} \ddot{x} \\ \ddot{y} \end{pmatrix} = \frac{U_z}{m} \begin{pmatrix} -s(\psi) & -c(\psi) \\ -s(\psi) & c(\psi) \end{pmatrix} \begin{pmatrix} \phi_{desired} \\ \theta_{desired} \end{pmatrix}$$
(11)

$$\begin{pmatrix} \phi_{desired} \\ \theta_{desired} \end{pmatrix} = \frac{m}{U_z} \begin{pmatrix} -s(\psi) & -c(\psi) \\ -s(\psi) & c(\psi) \end{pmatrix}^{-1} \begin{pmatrix} \ddot{x} \\ \ddot{y} \end{pmatrix}$$
(12)

The main objective of the nonlinear controller is to get the error of x and y positions approach zero as shown below:

$$\begin{cases} \ddot{x}_{desired} - \ddot{x}_{actual} + f_1(e_x) + f_2(\dot{e}_x) + f_3(\int e_x \, dt) \\ = 0 \\ \ddot{y}_{desired} - \ddot{y}_{actual} + f_1(e_y) + f_2(\dot{e}_y) + f_3(\int e_y \, dt) \\ = 0 \end{cases}$$
(13)

Sub. \ddot{x}_{actual} , \ddot{y}_{actual} of (13) into (12), yields,

$$\begin{pmatrix} \phi_{desired} \\ \theta_{desired} \end{pmatrix} = \frac{m}{U_z} \begin{pmatrix} -s(\psi) & -c(\psi) \\ -s(\psi) & c(\psi) \end{pmatrix}^{-1} \times \begin{pmatrix} \ddot{x}_{desired} + f_1(e_x) + f_2(\dot{e}_x) + f_3(\int e_x dt) \\ \ddot{y}_{desired} + f_1(e_y) + f_2(\dot{e}_y) + f_3(\int e_y dt) \end{pmatrix}$$

$$(14)$$

Assuming $\ddot{x}_{desired}$ and $\ddot{y}_{desired} = 0$. One obtains,

$$\begin{pmatrix} \phi_{desired} \\ \theta_{desired} \end{pmatrix} = \frac{m}{U_z} \begin{pmatrix} -s(\psi) & c(\psi) \\ -s(\psi) & -c(\psi) \end{pmatrix} \begin{pmatrix} U_x \\ U_y \end{pmatrix} (15)$$

The Overall controlled quadrotor system is shown in Fig. 4.

4.2 Stability Analysis of the closedloop system

In this section, the overall stability analysis of both the ILC and OLC systems will be demonstrated using Lyapunov principle. Before proceeding, some assumptions are needed.

Assumption 1. In order to prove the stability of the quadrotor system all α ,s in (6) will be approximated to 1 for the six controllers, because we designed the controller with almost $\alpha \approx 1$ (i.e. $|\beta| \operatorname{sign}(\beta) = \beta$).

Assumption 2. $I_x = I_y \approx I_z$ this assumption holds for small difference between $I_x, I_y \& I_z$.

Assumption 3. ϕ, θ and ψ are small enough, so that we can approximate $\sin(\beta) \approx \beta .\cos(\beta) \approx 1$.

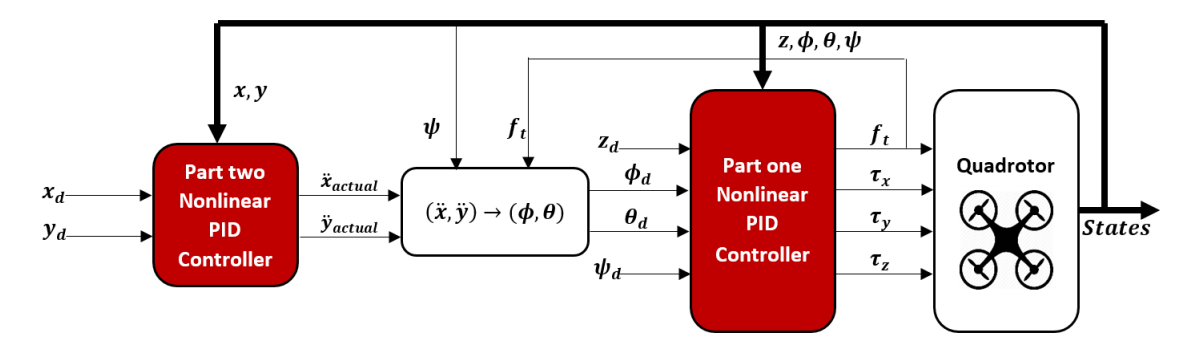


Figure 4: Overall Quadrotor system

4.2.1 Rotational dynamics stability

Theorem 1. The nonlinear PID controller proposed in (8)–(10) for ϕ , θ , and ψ in the last six equations of (3) under Assumption 2 and using the controllers (8)–(10) with Assumption 1, the rotational closed-loop system is stable and has a bounded error.

Proof. To prove Theorem 1 we used the following candidate Lyapunov function V and assumed the desired values are constant.

$$\begin{array}{l} V = \frac{1}{2}e_{\phi_0}^2 + \frac{1}{2}e_{\phi}^2 + \frac{1}{2}e_p^2 + \frac{1}{2}e_{\theta}^2 + \frac{1}{2}e_q^2 + \frac{1}{2}e_{\psi_0}^2 \\ + \frac{1}{2}e_{\psi}^2 + \frac{1}{2}e_r^2, V \geq 0 \end{array}$$

Where: $\sigma = \phi, \theta, \psi; \gamma = p, q, r; e_{\sigma_0} = \int_0^t e_{\sigma} d\tau, e_{\sigma} = \sigma_{desired} - \sigma; e_{\gamma} = -\gamma$

$$\dot{V} = e_{\phi_0} \dot{e}_{\phi_0} + e_{\phi} \dot{e}_{\phi} + e_p \dot{e}_p + e_{\theta} \dot{e}_{\theta} + e_q \dot{e}_q + e_{\psi_0} \dot{e}_{\psi_0} + e_{\psi} \dot{e}_{\psi} + e_r \dot{e}_r$$

$$\dot{V} = e_{\phi_0} e_{\phi} - e_{\phi} \dot{\phi} - e_p \dot{p} - e_{\theta} \dot{\theta} - e_q \dot{q} + e_{\psi_0} e_{\psi} - e_{\psi} \dot{\psi} - e_r \dot{r}$$

$$\dot{V} = E^T M E$$

Where :
$$E^T = [e_{\phi_0} e_{\phi} e_p e_{\theta_0} e_{\theta} e_q e_{\psi_0} e_{\psi} e_r]$$
, $M = \begin{bmatrix} 0 & 0 & -b_{\phi}f_{\phi 3} & 0 & 0 & 0 & 0 & 0 & 0 \\ 1 & 0 & -b_{\phi}f_{\phi 1} & 0 & 0 & 0 & 0 & 0 & 0 & 0 \\ 0 & 1 & -b_{\phi}f_{\phi 2} & 0 & 0 & -b_{\phi}f_{\phi 2}s\phi t\theta & 0 & 0 & -b_{\phi}f_{\phi 2}c\phi t\theta \\ 0 & 0 & 0 & 0 & 0 & -b_{\theta}f_{\theta 3} & 0 & 0 & 0 \\ 0 & 0 & 0 & 0 & 0 & -b_{\theta}f_{\theta 1} & 0 & 0 & 0 \\ 0 & 0 & 0 & 0 & 0 & -b_{\theta}f_{\theta 1} & 0 & 0 & 0 \\ 0 & s\phi t\theta & 0 & 0 & c\phi & -b_{\theta}f_{\theta 2}c\phi & 0 & \frac{s\phi}{c\theta} & b_{\theta}f_{\theta 2}s\phi \\ 0 & 0 & 0 & 0 & 0 & 0 & 0 & 0 & -b_{\psi}f_{\psi 3} \\ 0 & 0 & 0 & 0 & 0 & 0 & 1 & 0 & -b_{\psi}f_{\psi 3} \\ 0 & 0 & 0 & 0 & 0 & 0 & 1 & 0 & -b_{\psi}f_{\psi 3} \\ 0 & c\phi t\theta & 0 & 0 & -s\phi & -b_{\psi}f_{\psi 2}\frac{s\phi}{c\theta} & 0 & \frac{c\phi}{c\theta} & -b_{\psi}f_{\psi 2}\frac{c\phi}{c\theta} \end{bmatrix}$
$$b_{\phi} = \frac{1}{I_x}; b_{\theta} = \frac{1}{I_y}; b_{\psi} = \frac{1}{I_z};$$

$$f_{ij}(\beta) = (k_{j1} + \frac{k_{j2}}{1 + exp(\mu_j \beta^2)}), i = \phi, \theta, \psi$$

By checking the definiteness of the matrix M using Symbolic Toolbox in MATLAB, the matrix

M is negative semi-definite with all the leading principal minors M_{ii} are equal to zero, except the third one, $M_{33} = -b_{\phi}f_{\phi3}$, which is always negative since $k_{j1} \leq f_{\sigma j} \leq (k_{j1} + \frac{k_{j2}}{2})$, then the closed-loop system is stable and its errors are bounded, i.e. e_{ϕ} , e_{θ} , e_{ψ} , e_{p} , e_{q} , and $e_{r} \leq \epsilon$; ϵ is a small value.

4.2.2 Translational dynamics stability

Referring to (3), under Assumption 3, the motion in the x, y, and z-directions are given as

$$\dot{x} = u, \dot{u} = U_x \tag{16}$$

$$\dot{y} = v, \dot{v} = U_y \tag{17}$$

$$\dot{z} = w, \dot{w} = -\frac{U_z}{m} \tag{18}$$

Theorem 2 below is concerned with the stability analysis of the translational quadrotor system.

Theorem 2. The simplified control system shown in (16)–(18) derived from (3) and (4) under Assumption 3 and using the controllers in (7) and (13) with Assumption 1, the translational closed-loop system is asymptotically stable.

Proof. We proceed in the proof by selecting the following candidate Lyapunov function V and assumed the desired values are constant.

$$V = \frac{1}{2}e_{\sigma 0}^2 + \frac{1}{2}e_{\sigma}^2 + \frac{1}{2}e_{\gamma}^2, V \ge 0$$

Where:
$$\sigma=x,y,-z;\gamma=u,v,-w;e_{\sigma 0}=\int_0^t e_\sigma\,d au,$$
 $e_\sigma=\sigma_{desired}-\sigma;e_\gamma=-\gamma$ $\dot{V}=e_{\sigma_0}\dot{e}_{\sigma_0}+e_\sigma\dot{e}_\sigma+e_\gamma\dot{e}_\gamma$ $\dot{V}=e_{\sigma_0}e_\sigma+e_\sigma e_\gamma-a_\sigma U_\sigma e_\gamma$ $\dot{V}=e_{\sigma_0}e_\sigma+e_\sigma e_\gamma-a_\sigma f_{\sigma 1}e_\sigma e_\gamma-a_\sigma f_{\sigma 2}\dot{e}_\sigma e_\gamma-a_\sigma f_{\sigma 3}e_{\sigma 0}e_\gamma$ $\dot{V}=e_{\sigma_0}e_\sigma+e_\sigma e_\gamma-a_\sigma f_{\sigma 1}e_\sigma e_\gamma-a_\sigma f_{\sigma 2}\dot{e}_\sigma^2-a_\sigma f_{\sigma 3}e_{\sigma 0}e_\gamma$ $\dot{V}=E_\sigma^TM_\sigma E_\sigma$ Where $:a_\sigma=1$ for $\sigma=y,z$ and $a_\sigma=\frac{1}{m}$ for $\sigma=z;E_\sigma^T=[e_{\sigma_0}\,e_\sigma\,e_\gamma]$ $M_\sigma=\begin{bmatrix}0&1&0\\0&0&1\\-a_\sigma f_{\sigma 3}&-a_\sigma f_{\sigma 1}&-a_\sigma f_{\sigma 2}\end{bmatrix}$ where: $f_{\sigma j}(\beta)=(k_{j1}+\frac{k_{j2}}{1+exp(\mu_j\beta^2)})$

The matrix M_{σ} is found to be negative definite by checking the eigenvalues using the formula $|\lambda I - M_{\sigma}| = 0$, we found $\lambda^3 + a_{\sigma} f_{\sigma 2} \lambda^2 + a_{\sigma} f_{\sigma 1} \lambda + a_{\sigma} f_{\sigma 3} = 0$, by using Routh-Hurwitz Criterion shown below:

$$\begin{array}{c|cccc}
\lambda^3 & 1 & a_{\sigma}f_{\sigma 1} \\
\lambda^2 & a_{\sigma}f_{\sigma 2} & a_{\sigma}f_{\sigma 3} \\
\lambda^1 & \frac{a_{\sigma}f_{\sigma 1}f_{\sigma 2} - f_{\sigma 3}}{f_{\sigma 2}} \\
\lambda^0 & a_{\sigma}f_{\sigma 3}
\end{array}$$

the conditions to keep the matrix M_{σ} negative definite are $a_{\sigma}f_{\sigma 1}, a_{\sigma}f_{\sigma 2}, a_{\sigma}f_{\sigma 3} > 0$ and $a_{\sigma}f_{1}f_{2} > f_{\sigma 3}$. The first condition is always true since $k_{j1} \leq f_{\sigma j} \leq (k_{j1} + \frac{k_{j2}}{2})$ and $a_{\sigma} > 0$ for all σ , while the second condition can be made always true by choosing the right values, then the translational closed-loop quadrotor system is asymptotically stable and thus its errors are bounded and goes to zero.

5 Simulation Results and Case Studies

5.1 Step reference tracking

The quadrotor dynamic model and the controller is implemented using MATLAB/Simulink and we have assumed that the wind forces and torques are negligible. The parameters values of the quadrotor used in the simulations are listed in Table 2. In these simulations, a comparison between the proposed nonlinear PID controller and a linear PID

controller is presented for each test. The parameters of both controllers $[(K_p, K_i, K_d)$: Linear PID; $(k_{i1}, k_{i2}, \mu_i, \alpha_i), i = 1, 2, 3$: Nonlinear PID] are tuned using GA according to the performance indices shown in Table 3.

Table 2: Parameters Values

Parameter	Value
I_x	8.5532×10^{-3}
$\overline{I_y}$	8.5532×10^{-3}
I_z	1.476×10^{-2}
\overline{g}	9.81
$\overline{}$	0.964
\overline{b}	7.66×10^{-5}
$\overline{}$	5.63×10^{-6}
$\overline{}$	0.22

Table 3: Performance Indices

Performance		Mathematical
Index	Description	Representa-
		tion
ITAE	Integrated time	$\int_0^{t_f} t e(t) dt$
	absolute error	
USQR	Controller	$\int_0^{t_f} [u(t)]^2 dt$
	energy	

 $*t_f$ is the final time of simulation

In order to tune the controllers using GA for optimization of the parameters of both controllers, a multi-objective function should be selected for the controllers of the 6-DOF quadrotor system. The general objective function that we used in our simulations is,

$$OPI_i = w_{1i} \times \frac{ITAE_i}{N_{1i}} + w_{2i} \times \frac{USQR_i}{N_{2i}}; i = x, y, z, \phi, \theta, \psi$$

$$(19)$$

Where: $w_{1i} + w_{2i} = 1$, weighting variables; N_{1i} and N_{2i} are normalizing variables. The weights w_{1i} , w_{2i} are defined as the relative emphasis of one objective as compared to the other. The values of w_{1i} , w_{2i} are chosen to increase the pressure on selected objective function. The N_{1i} and N_{2i} are included in the performance index to insure that the individual objectives have comparable values, and are treated

equally likely by the tuning algorithm. Because, if a certain objective is of very high value, while the second one has very low value, then the tuning algorithm will pay much consideration to the highest one and leave the other with little reflection on the system.

The values of both controllers after tuning are listed in Tables 4 and 5. After tuning the overall quadrotors six controllers, the performance indices for $(x, y, z, \text{ and } \psi)$ and the quadrotor total OPI are shown in Table 6.

Table 4: LPID Parameters

	$\overline{k_p}$	k_i	k_d
\overline{x}	0.28	2.73×10^{-6}	0.63
\overline{y}	0.36	1.56×10^{-5}	0.88
\overline{z}	184.02	103.73	22.5
$\overline{\phi}$	0.88	0.9	0.3
θ	0.62	0.81	0.05
$\overline{\psi}$	0.99	0.49	0.56

Table 5: NLPID Parameters

	x	y	z	ϕ	θ	ψ
k_{11}	1.51	1.38	27.5	0.77	0.48	0.76
k_{12}	0.04	0.03	8.76	0.06	0.03	0.16
k_{21}	1.13	2.51	8.8	0.2	0.08	0.17
k_{22}	0.18	0.04	4.71	0.04	0.12	0.11
k_{31}	1.81×	$5.72 \times$	18.49	1.08	0.88	0.27
	10^{-6}	10^{-5}				
k_{32}	10^{-6}	$8.69 \times$	10.02	0.08	0.11	0.08
		10^{-6}				
$\overline{\mu_1}$	0.11	0.08	0.31	0.07	0.84	0.25
μ_2	0.08	0.36	0.36	0.56	1.43	0.46
μ_3	0.18	0.6	0.98	0.58	0.28	0.81
α_1	0.93	0.93	0.96	0.96	0.96	0.98
α_2	0.93	0.92	0.97	0.96	1	0.95
α_3	0.95	0.93	0.97	0.97	0.97	0.92

Table 6: Position and Yaw Performance indices

	LPID		NLPID	
	ITAE	ISU	ITAE	ISU
\overline{x}	14.285931	0.134411	0.438883	0.381936
\overline{y}	7.498694	0.323482	1.066173	1.226223
z	0.059225	5197.496	0.152148	4516.303
$\overline{\psi}$	1.377493	0.030779	0.506028	0.037517
OPI	3.949482		0.40	1934

A unit step reference inputs $(x_{desired}, y_{desired}, z_{desired},$ and $\psi_{desired})$ have been applied to the position (x, y,and z) of the 6-DOF and the yaw (ψ)

orientation. the curves in Fig. 5 (a), represent the response of the x-position of the quadrotor system using both controllers, while (b) represent the energy signal produced by the controllers to achieve the required position. The output response for y, z, and ψ are shown in Figs. 6–8. As can be seen from these Figures, the control signal produced by the nonlinear PID controller is less fluctuating than that in the linear PID controller. The nonlinear PID controller shows a faster response than the linear PID one, except for the z-position, where the linear PID controller presents a faster tracking, but on the account of a large control energy being spent for this fast tracking. This increase in the energy of the control signal is undesired in the practice, since it leads to actuator saturation. The overshoot in the output response for the PID controller is very clear. The output responses of ϕ and θ are drawn in Figs. 9 and 10 which shows the effectiveness of the proposed nonlinear controller over the linear PID one. This has been definitely reflected on the energy of the control signal and the smoothness of the output response. the energy signals for ϕ and θ showed a huge difference in their responses.

The time-domain specifications of both controllers are presented numerically in Table 7 (rising t_r , settling t_s and peak overshot M_p) for the position (x, y, and z) of the quadrotor system and yaw (ψ) using both controllers. Table 8 shows the minimum and maximum peaks for ϕ and θ using both controllers.

Table 7: Position and Yaw responses

	LPID			NLPID		
	$t_r(s)$	$t_s(s)$	$M_p\%$	$t_r(s)$	$t_s(s)$	$M_p\%$
x	6.546	13.679	7.471	1.152	4.657	0.505
y	1.934	9.748	19.375	1.572	3.023	0.195
z	0.194	0.314	1.531	0.677	1.283	0.505
ψ	0.681	5.660	19.014	0.252	3.840	8.152

Table 8: Roll and Pitch responses

	LPII	D	NLPID	
	Min peak	Max	Min peak	Max
		peak		peak
$\overline{\theta}$	$-8.292 \times$	$3.91 \times$	$-3.951 \times$	$7.402 \times$
	10^{-2}	10^{-1}	10^{-2}	10^{-2}
$\overline{\psi}$	$-9.195 \times$	$4.385 \times$	$-3.775 \times$	$1.065 \times$
	10^{-1}	10^{-1}	10^{-1}	10^{-1}

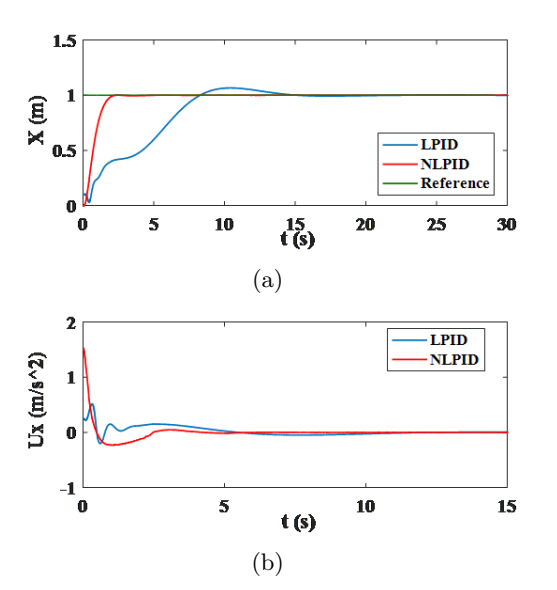


Figure 5: x-position (a) time response (b) controller signal

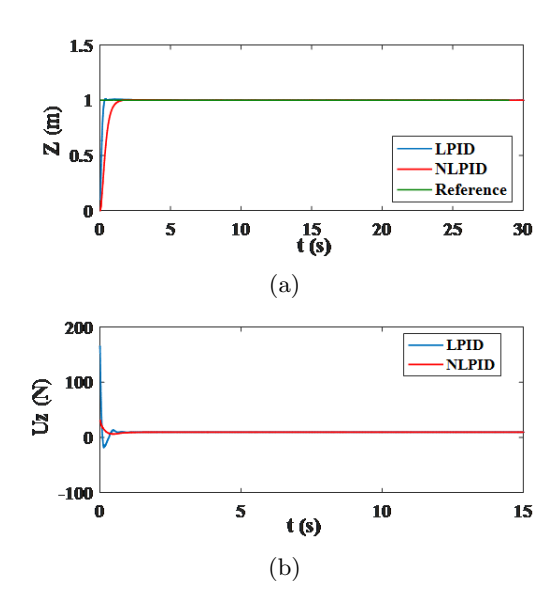


Figure 7: z-position (a) time response (b) controller signal

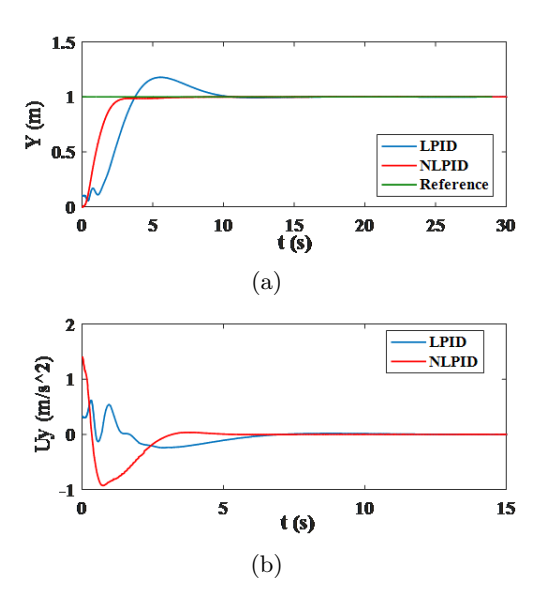


Figure 6: y-position (a) time response (b) controller signal

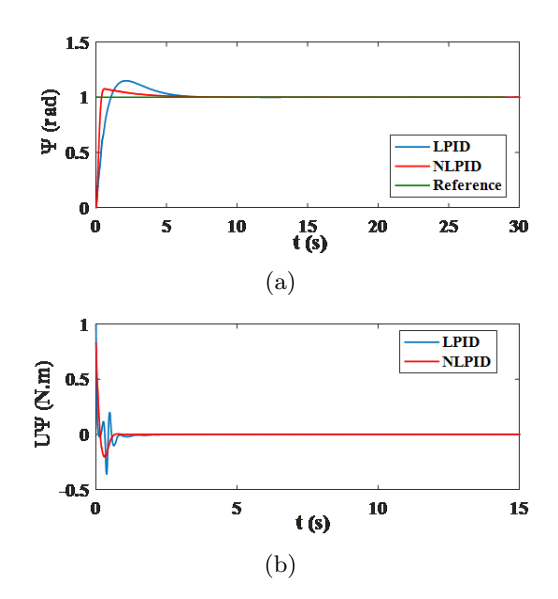


Figure 8: ψ -position (a) time response (b) controller signal

5.2 Trajectory tracking

In the following, the output responses of three case studies with trajectories generated by MAT-LAB/Simulink to test the overall 6-DOF UAV system using Linear and Nonlinear PID controllers will

be presented and discussed. The cases studied have been chosen to reflect the difficulties that the quadcopter control system might face in achieving the required tracking. For all of the case studies, the initial values are x=0.1,y=0.1,z=0.1 and the rest of the states are zero.

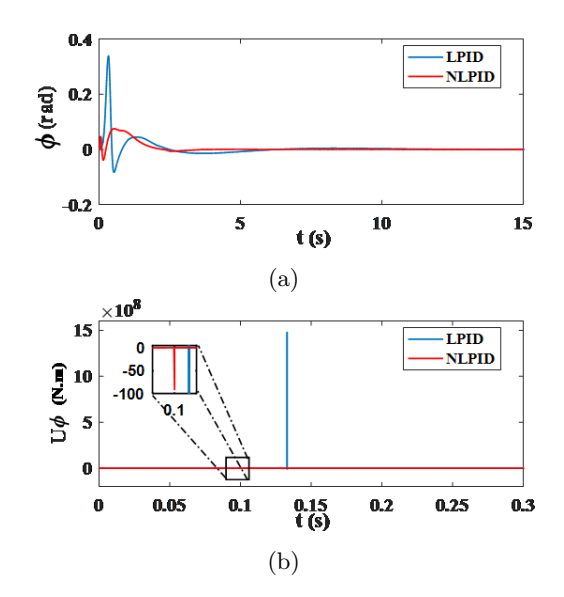


Figure 9: ϕ -position (a) time response (b) controller signal

Case Study (1). The first test case study was the circular path. The States with the reference trajectories are presented in Table 9.

Table 9: Case 1 input signals

State	Reference Trajectory	Time/sec		
x	$cos(0.1\pi t)$	$5-t_f$		
y	$sin(0.1\pi t)$	$5-t_f$		
\overline{z}	u(t)	$0-t_f$		
$\overline{\psi}$	u(t)	$0-t_f$		
$*t_f = 50sec$				

Fig. 11 shows the tracking of the 6-DOF UAv system for the circular trajectory. The proposed Nonlinear PID controller followed the trajectory with less time and smaller error than in the Linear PID one. The steady state error in the linear PID controller was $e_x=27\%, e_y=18\%,$ and $e_z=0\%$, while in the proposed nonlinear PID controller the steady state error was $e_x=0.56\%, e_y=4.12\%,$ and $e_z=0\%.$

Case Study (2). The Second test case was the helical path, in this case study the altitude z of the 6-DOF UAV is varying with time, in contrast to the first case study. The States with reference trajectories are presented in Table 10.

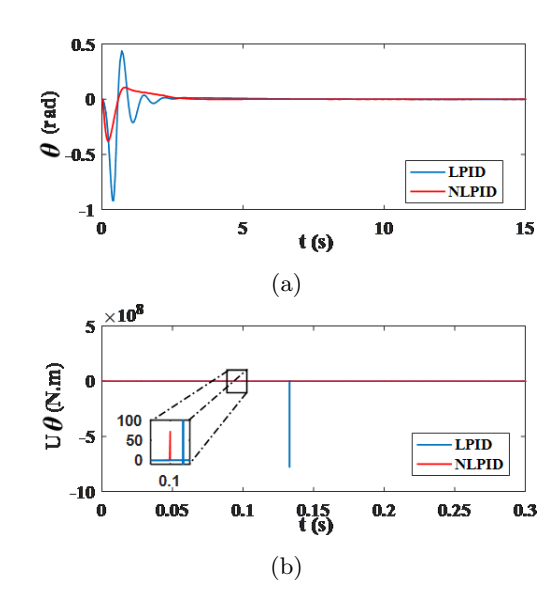


Figure 10: θ -position (a) time response (b) controller signal

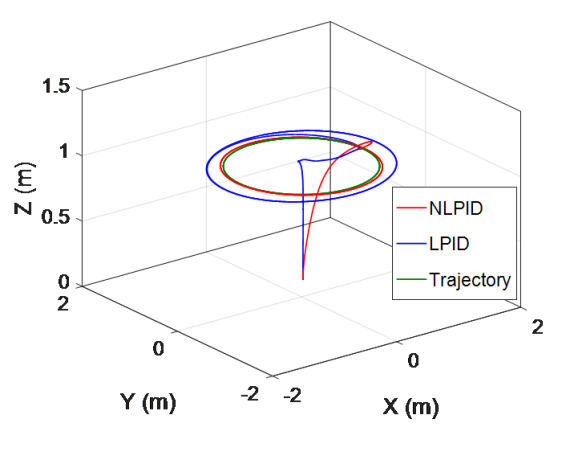


Figure 11: Case 1 Trajectory

Table 10: Case 2 input signals

State	Reference Trajectory	Time/sec	
\overline{x}	$cos(0.1\pi t)$	$5-t_f$	
\overline{y}	$sin(0.1\pi t)$	$5-t_f$	
\overline{z}	0.2t	$0-t_f$	
$\overline{\psi}$	u(t)	$0-t_f$	
$*t_f = 100sec$			

The linear PID controller follows the desired trajectory with constant offset for the entire time of the simulations. While the proposed nonlinear PID controller showed an improved performance over the linear PID one as shown in Fig. 12.

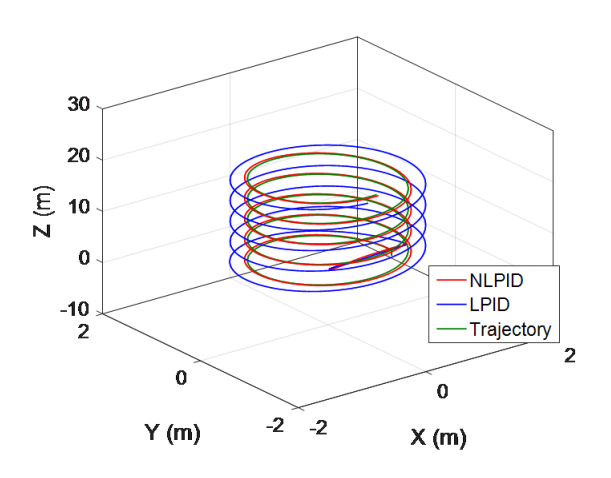


Figure 12: Case 2 Trajectory

Case Study (3). The final case study is the square trajectory. This trajectory is a serious test for the controllers designed for the UAV systems to accomplish the required track, since, the trajectory changes its direction suddenly at certain times (i.e., at the vertices of the square). States with functions are in Table 11.

Table 11: Case 3 input signals

		-
State	Reference Trajectory	Time/sec
\overline{x}	u(t-10) - u(t-50)	10 - 50
\overline{y}	(t-30) - u(t-70)	30 - 70
\overline{z}	u(t)	$0-t_f$
$\overline{\psi}$	u(t)	$0-t_f$
	$*t_{c} = 100 sec$	

We can see the difference between the responses of both controllers in Fig. 13. The significance of the Nonlinear PID controller is very obvious, it tracked faster than the linear PID one with very small overshot as compared to the Linear PID controller. The overshot in the Linear PID reached approximately up to 200% of the desired trajectory.

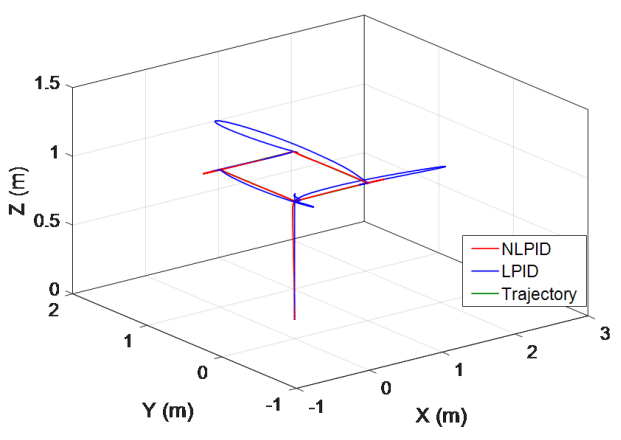


Figure 13: Case 3 Trajectory

6 Conclusion and Future Work

In this work, the exact nonlinear model of the 6-DOF UAV was adopted with the aim of designing a nonlinear controller for the stabilization and reference tracking for this complex and highly nonlinear system. A new nonlinear PID controller for stabilizing and controlling a 6-DOF UAV system is proposed in this paper. The stability analysis for the closed-loop systems of both the position and orientation of the 6-DOF UAV system based on Lyapunov method was analyzed and proved that the purposed controller stabilized the system and accomplished the required tracking. From the simulation tests, it can be concluded that the proposed nonlinear PID controller is better than the linear PID one in terms of speed, control energy, and steady state error. For future work, we suggest taking wind disturbances into account and rejecting them by designing a disturbance observer using active disturbance rejection control paradigm for this purpose.

Acknowledgment

Authors deeply thank Electrical Engineering Department/College of Engineering/Baghdad University for providing the online library. Also, special thanks go to the Ph.D. student Wameedh R. Abdul-Adheem for the deep discussions on the top-

ics of this paper.

References

- P. V. Kumar, A. Challa, J. Ashok, and G. L. Narayanan, "GIS based fire rescue system for industries using Quad copter A novel approach," in 2015 International Conference on Microwave, Optical and Communication Engineering (ICMOCE), pp. 72–75, IEEE, dec 2015.
- [2] O. I. Dallal Bashi, W. Z. Wan Hasan, N. Azis, S. Shafie, and H. Wagatsuma, "Quadcopter sensing system for risky area," in 2017 IEEE Regional Symposium on Micro and Nanoelectronics (RSM), pp. 216–219, IEEE, aug 2017.
- [3] H. Saha, S. Basu, S. Auddy, R. Dey, A. Nandy, D. Pal, N. Roy, S. Jasu, A. Saha, S. Chattopadhyay, and T. Maity, "A low cost fully autonomous GPS (Global Positioning System) based quad copter for disaster management," in 2018 IEEE 8th Annual Computing and Communication Workshop and Conference (CCWC), no. 0, pp. 654–660, IEEE, jan 2018.
- [4] J. Navia, I. Mondragon, D. Patino, and J. Colorado, "Multispectral mapping in agriculture: Terrain mosaic using an autonomous quadcopter UAV," in 2016 International Conference on Unmanned Aircraft Systems (ICUAS), pp. 1351–1358, IEEE, jun 2016.
- [5] R. Daroya and M. Ramos, "NDVI image extraction of an agricultural land using an autonomous quadcopter with a filter-modified camera," in 2017 7th IEEE International Conference on Control System, Computing and Engineering (ICCSCE), no. 0, pp. 110–114, IEEE, nov 2017.
- [6] G. Hunt, F. Mitzalis, T. Alhinai, P. A. Hooper, and M. Kovac, "3D printing with flying robots," in 2014 IEEE International Conference on Robotics and Automation (ICRA), pp. 4493–4499, IEEE, may 2014.
- [7] E. Camci and E. Kayacan, "Waitress quadcopter explores how to serve drinks by reinforcement learning," in 2016 IEEE Region 10

- Conference (TENCON), pp. 28–32, IEEE, nov 2016.
- [8] S. J. Kim, Y. Jeong, S. Park, K. Ryu, and G. Oh, "A Survey of Drone use for Entertainment and AVR (Augmented and Virtual Reality)," in Augmented Reality and Virtual Reality (T. Jung and M. C. tom Dieck, eds.), Progress in IS, pp. 339–352, Cham: Springer International Publishing, 2018.
- [9] A. Eskandarpour and V. J. Majd, "Cooperative formation control of quadrotors with obstacle avoidance and self collisions based on a hierarchical MPC approach," in 2014 Second RSI/ISM International Conference on Robotics and Mechatronics (ICRoM), pp. 351–356, IEEE, oct 2014.
- [10] A. Rabah and W. Qing-he, "Adaptive leader follower control for multiple quadrotors via multiple surfaces control," *Journal of Beijing Institute of Technology (English Edition)*, vol. 25, no. 4, pp. 526–532, 2016.
- [11] K. A. Ghamry and Y. Zhang, "Cooperative control of multiple UAVs for forest fire monitoring and detection," in 2016 12th IEEE/ASME International Conference on Mechatronic and Embedded Systems and Applications (MESA), pp. 1–6, IEEE, aug 2016.
- [12] Z. Hou, W. Wang, G. Zhang, and C. Han, "A survey on the formation control of multiple quadrotors," in 2017 14th International Conference on Ubiquitous Robots and Ambient Intelligence (URAI), pp. 219–225, IEEE, jun 2017.
- [13] D. Kotarski, Z. Benic, and M. Krznar, "Control Design for Unmanned Aerial Vehicles with Four Rotors," *Interdisciplinary Description of Complex Systems*, vol. 14, no. 2, pp. 236–245, 2016.
- [14] N. Hadi and A. Ramz, "Tuning of PID Controllers for Quadcopter System using Hybrid Memory based Gravitational Search Algorithm Particle Swarm Optimization," International Journal of Computer Applications, vol. 172, pp. 9–18, aug 2017.

- [15] M. Akhil, M. K. Anand, A. Sreekumar, and P. Hithesan, "Simulation of the Mathematical Model of a Quad Rotor Control System Using Matlab Simulink," *Applied Mechanics* and Materials, vol. 110-116, pp. 2577–2584, oct 2011.
- [16] M. A. Alsharif, Y. E. Arslantas, and M. S. Holzel, "A comparison between advanced model-free PID and model-based LQI attitude control of a quadcopter using asynchronous android flight data," in 2017 25th Mediterranean Conference on Control and Automation (MED), pp. 1023–1028, IEEE, jul 2017.
- [17] S. Gonzalez-Vazquez and J. Moreno-Valenzuela, "A New Nonlinear PI/PID Controller for Quadrotor Posture Regulation," in 2010 IEEE Electronics, Robotics and Automotive Mechanics Conference, pp. 642–647, IEEE, sep 2010.
- [18] R. R. Benrezki, M. Tadjine, F. Yacef, and O. Kermia, "Passive fault tolerant control of quadrotor UAV using a nonlinear PID," in 2015 IEEE International Conference on Robotics and Biomimetics (ROBIO), pp. 1285–1290, IEEE, dec 2015.
- [19] L. M. Argentim, W. C. Rezende, P. E. Santos, and R. A. Aguiar, "PID, LQR and LQR-PID on a quadcopter platform," in 2013 International Conference on Informatics, Electronics and Vision (ICIEV), pp. 1–6, IEEE, may 2013.
- [20] T. Lee, M. Leok, and N. H. McClamroch, "Geometric tracking control of a quadrotor UAV on SE(3)," in 49th IEEE Conference on Decision and Control (CDC), vol. 15, pp. 5420–5425, IEEE, dec 2010.
- [21] P. Ru and K. Subbarao, "Nonlinear Model Predictive Control for Unmanned Aerial Vehicles," *Aerospace*, vol. 4, pp. 1–26, jun 2017.
- [22] K. M. Thu and A. Gavrilov, "Designing and Modeling of Quadcopter Control System Us-

- ing L1 Adaptive Control," *Procedia Computer Science*, vol. 103, no. October 2016, pp. 528–535, 2017.
- [23] E. A. Seidabad, S. Vandaki, and A. V. Kamyad, "Designing Fuzzy PID Controller for Quadrotor," International Journal of Advanced Research in Computer Science & Technology (IJARCST 2014), vol. 2, no. 4, pp. 221–227, 2014.
- [24] Eduardo M. Bucio-Gallardo, Ricardo Zavala-Yoé, and Ricardo A. Ramírez-Mendoza, "Mathematical Model and Intelligent Control of a Quadcopter, with Non-conventional Membership Functions," *Journal of Energy and Power Engineering*, vol. 10, pp. 634–642, oct 2016.
- [25] A. Zulu and S. John, "A Review of Control Algorithms for Autonomous Quadrotors," *Open Journal of Applied Sciences*, vol. 04, no. 14, pp. 547–556, 2014.
- [26] W. Riyadh and I. Kasim, "From PID to Nonlinear State Error Feedback Controller," International Journal of Advanced Computer Science and Applications, vol. 8, no. 1, pp. 312– 322, 2017.
- [27] A. T. Nugraha and T. Agustinah, "Quadcopter path following control design using output feedback with command generator tracker based on LOS," in 2017 International Seminar on Intelligent Technology and Its Applications (ISITIA), vol. 947, pp. 255–260, IEEE, aug 2017.
- [28] F. Sabatino, Quadrotor control: modeling, nonlinear control design, and simulation. Master's thesis, Royal Institute of Technology, 2015.
- [29] R. W. Beard, "Quadrotor Dynamics and Control," *Brigham Young University*, no. June, pp. 1–47, 2008.